



Role of ADC map MR imaging in prediction of local aggressiveness of prostate cancer

A THESIS SUBMITTED FOR PARTIAL FULFILMENT
OF MASTER DEGREE IN RADIOLOGY

Presented by

Asaad Gamal Asaad Sorial

M.B.B.CH. – Ain Shams University

Supervised by

Prof. Mohsen Gomaa Hassan Ismail

Professor of Radiodiagnosis

Faculty of Medicine

Ain Shams University

Dr. Omar Farouk Kamel

Lecturer of Radiodiagnosis

Faculty of Medicine

Ain Shams University

Faculty of Medicine

Ain Shams University

2018

ACKNOWLEDGEMENT

*First, I thank **God** for blessing me more than I deserve and for his uncountable gifts which are exceeding abundantly above all what we ask or think,*

*I would like to express my deepest appreciation and gratitude to **Prof. Dr. Mohsen Gomaa Hassan Ismail** for his sincere encouragement, constant advice and gentle dealing with me like a father with his son, it is a real honor for me to work under his supervision.*

*I owe special thanks, gratitude and appreciation to **Lecturer. Dr. Omar Farouk Kamel** for his close supervision, continuous advice and support which gave me the best guidance during different stages of this work.*

*I must express by profound gratitude to my **father** and **mother** for providing everything. I can't repay them.*

Last but not least I thank my friends and colleagues in the Radiology department of Ain Shams University for helping me in many ways throughout my residency.



دورالرنين المغناطيسى باستخدام خريطة معامل الانتشار الظاهرية فى توقع عدوانية سرطان البروستاتا

رسالة

توطئة للحصول على درجة الماجستير فى الأشعة التشخيصية

مقدمة من

طبيب / أسعد جمال أسعد سوريال

بكالوريوس الطب والجراحة – جامعة عين شمس

وذلك تحت إشراف

أ.د/ محسن جمعة حسن إسماعيل

أستاذ الاشعة التشخيصية

كلية الطب- جامعة عين شمس

د/ عمر فاروق كامل

مدرس الاشعة التشخيصية

كلية الطب- جامعة عين شمس

كلية الطب
جامعة عين شمس

2018

INDEX

LIST OF FIGURES	II
LIST OF TABLES	IV
LIST OF ABBREVIATIONS	V
INTRODUCTION	1
AIM OF WORK	3
ANATOMY OF THE PROSTATE	4
PATHOLOGY OF PROSTATE CANCER	25
MRI APPEARANCE OF PROSTATE CANCER	47
DIFFUSION MRI PRINCIPLES	57
APPLICATIONS OF DWI IN PROSTATE CANCER	69
PATIENTS AND METHODS	81
RESULTS	85
ILLUSTRATED CASES	93
DISCUSSION	100
SUMMARY AND CONCLUSION	111
REFERENCES	112

List of figures		
Figure 1	Diagrammatic representation of the pelvic Anatomy	5
Figure 2	Diagram of the lobar and zonal anatomy of the prostate	6
Figure 3	Diagrammatic representation showing different zones	11
Figure 4	Zonal anatomy of the prostate in Young versus older males	14
Figure 5	The European Consensus Guidelines division of the prostate	17
Figure 6	Diagram showing the arterial Supply of the Prostate	18
Figure 7	Diagram showing the venous Drainage of the Prostate	19
Figure 8	Diagram showing distribution of nerve branches to the prostate	21
Figure 9	Normal MRI prostate zonal anatomy	24
Figure 10	Original Gleason score	31
Figure 11	Prostate carcinoma with cribriform glands	36
Figure 12	the TNM staging of prostatic carcinoma	46
Figure 13	Stating of the prostate cancer	50
Figure 14	example of extracapsular spread	51
Figure 15	PI-RADS classification of prostate cancer	56
Figure 16	Diffusion of water molecules	58
Figure 17	diagrammatic representation of measuring water diffusion	61
Figure 18	T2 shine-through effect with DWI	64
Figure 19	MRI of a case of BPH	70
Figure 20	MRI of a case of prostate cancer	71

List of figures (cont.)		
Figure 21	MRI of a case of prostate cancer with extracapsular invasion	73
Figure 22	MRI of a case of prostate cancer yet no extracapsular invasion	74
Figure 23	MRI of a case of prostate cancer with hemorrhage after biopsy	75
Figure 24	MR imaging–guided prostate biopsy	77
Figure 25	MRI of a case after radical retropubic prostatectomy	79
Figure 26	response in prostate cancer before and after radiation	80
Figure 27	Chart demonstrating the site of the prostate cancer	86
Figure 28	Pie chart demonstrating percentage of positive T2 in localization of prostate cancer	86
Figure 29	Pie chart demonstrating percentage of positive DWI in localization of prostate cancer	87
Figure 30	Chart demonstrating the difference between T2, DWI and ADC map images in localization of the lesions	87
Figure 31	chart demonstrating Gleason score representation among patients	88
Figure 32	demonstrating the relationship between the mean ADC value and the Gleason score	89
Figure 33	Demonstrating the relationship between the mean ADC value and the grade of the tumor	90
Figure 34	Chart demonstrating the relation chip between the mean ADC value and Gleason scores 3+4 and 4+3	91
Figure 35	illustrative case I	93
Figure 36	illustrative case II	94
Figure 37	illustrative case III	95
Figure 38	illustrative case IV	96
Figure 39	follow up MRI of illustrative case IV	97
Figure 40	illustrative case V	98
Figure 41	follow up MRI of illustrative case V	99

List of tables		
Table 1	make up of the normal prostate gland	8
Table 2	New grading system for prostate cancer	37
Table 3	PI-RADS score: Definition of total score and assignment	56
Table 4	Demonstrating the PSA and age of the patients.	85
Table 5	the mean ADC value and the SD of each GS	88
Table 6	the mean ADC value and the SD of different grades of the tumor	89
Table 7	Demonstrating the difference between the mean ADC value and the standard deviation of Gleason score 3+4 and Gleason score 4+3	91
Table 8	Demonstrating the results of the ROC for Gleason score >7	92
Table 9	Demonstrating the results of the ROC for Gleason score <7	92
Table 10	Published data on Gleason Score (GS) and ADC Values	103

List of abbreviations	
AAH	Atypical adenomatous hyperplasia
ADC	Apparent diffusion coefficient
BIRADS	Breast imaging reporting and data system
BPH	Benign prostatic hyperplasia
CT	Computed tomography
CZ	Central zone
DCE-MRI	Dynamic contrast enhanced magnetic resonance imaging
DRE	Digital rectal examination
DWI	Diffusion weighted imaging
DW-MRI	Diffusion weighted magnetic resonance imaging
ECE	Extra capsular extension
ECS	Extracellular space
GS	Gleason score
HIFU	High intensity focused ultrasound
ICS	Intracellular space
ISUP	International society of urological pathology
LN	Lymph node
MR	Magnetic resonance
MRI	Magnetic resonance imaging
MRS	Magnetic resonance spectroscopy
PCa	Prostate cancer
PIN	Prostatic intraepithelial neoplasia
PIRADS	Prostate imaging reporting and data system
PSA	Prostatic specific antigen
PSAD	Prostatic specific antigen density
PSAV	Prostatic specific antigen velocity
PZ	Peripheral zone
RF	Radiofrequency
ROI	Region of interest
SVI	Seminal vesicle invasion
TRUS	Transrectal ultrasound
TZ	Transitional zone
US	Ultrasound
WHO	World health organization

Introduction

Prostate cancer is the most commonly diagnosed solid malignant tumor among men. The morbidity and mortality directly attributable to this common malignancy are significant. However, in a non negligible proportion of patients, the disease may be considered relatively indolent. **(De Cobelli et al., 2015).**

The diagnosis of prostate cancer is based on a digital rectal examination (DRE) and assessment of serum prostate specific antigen (PSA) followed by transrectal ultrasound (TRUS)-guided biopsy. **(Anwar et al., 2014).**

T2-weighted MRI has been commonly used to detect prostate cancer. Recently, diffusion-weighted MRI (DW-MRI) has been widely introduced in the clinical setting. It is beneficial as it offers increased diagnostic accuracy due to the clear delineation between normal and prostate cancer, namely the high signal of cancerous lesions. DW-MRI is a non-invasive imaging technique that quantifies the diffusion of water molecules in tissues without any contrast agents, tracers, or exposure to radiation. DW-MRI may also provide qualitative information

regarding the pathophysiological character of prostate cancer. **(Bae et al.,2014).**

The assessment of local aggressiveness of prostate cancer (PCa) is of key importance for appropriate management of this disease. The increase in life expectancy of the general population combined with efficient screening methods will lead to an increase in the number of new PCa cases. These cases will tend to be more localized and at an earlier stage. **(Lebovici et al., 2014).**

The Gleason scoring (GS) system has been accepted internationally as a reference grading system for prostate cancer with respect to tumor aggressiveness, tumors are classified as low risk (Gleason score, ≤ 6), intermediate risk (Gleason score, 7) or high risk (Gleason score, ≥ 8). **(Doo et al., 2012).**

To establish the ADC as a strong biomarker for predicting prostate cancer Gleason scores, standardization of quantitative ADC metrics is of crucial importance. **(Donati et al., 2014).**

Aim of work

The objective of this study is to evaluate the relationship between ADC map values of MR imaging and local aggressiveness of the prostate cancer via comparing the ADC values and Gleason score in prostate cancer.

ANATOMY OF THE PROSTATE

The prostate gland is the largest of the accessory reproductive glands; it is located retroperitoneally in the pelvis posterior to the inferior border of the symphysis pubis (**McGee et al., 1992**).

The prostate is an ovoid structure resembling an inverted bilobed cone, located between the urinary bladder superiorly and the pelvic floor inferiorly. The urethra traverses it, entering at the broad base of the cone just below the bladder neck and exiting near the narrowed apex of the cone at the level of the urogenital diaphragm. The rounded anterior surface is behind the pubis and the posterior surface is flattened with a midline depression (the median sulcus) that lies against the rectal ampulla. The lateral and inferior surfaces of the gland are in contact with the levator ani muscles. The ejaculatory ducts enter the posterior surface laterally and pass obliquely toward the midline, where they end at the verumontanum on the posterior surface of the prostatic urethra (**Rogers et al., 2002**).

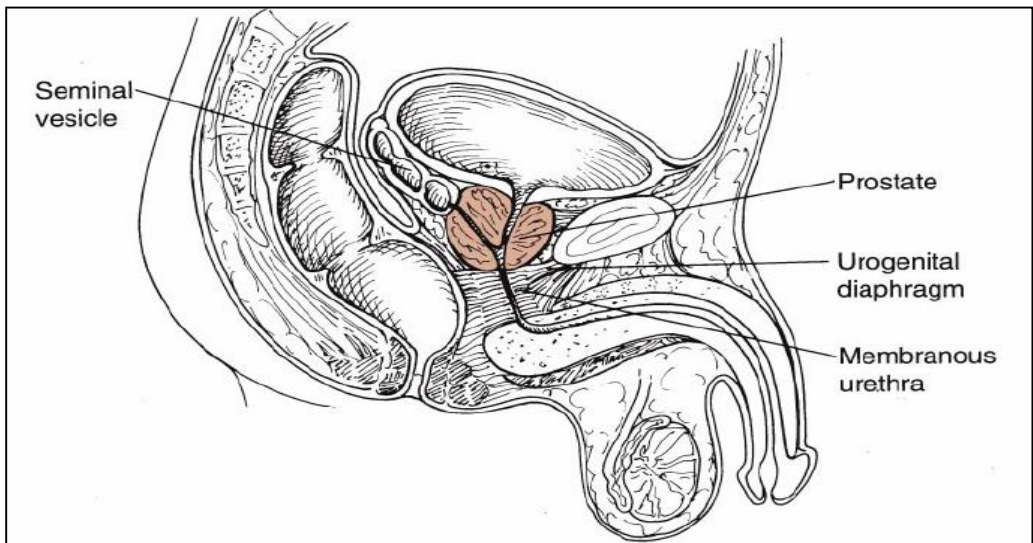


Figure 1 : Diagrammatic representation of the pelvic Anatomy.
(Rogers et al., 2002).

Prostate was described previously as consisting of a number of ill-defined lobes. However, this terminology has been replaced by the concept of prostate zones and segments.

Lobar Anatomy

According to **Lowsley 1912**, the prostate can be divided into five lobes. Anterior to urethra lies the isthmus or the anterior lobe, which contains fibro-muscular tissue and little amount of glandular tissue. Posterior to the urethra and inferior to the ejaculatory ducts is posterior lobe that can be palpated by rectal examination. Its ducts end below the ejaculatory ducts in posterior wall of the urethra. The lateral lobes form the major part of prostate on either side of the urethra. Their ducts end in the lateral grooves of the urethra. The median lobe is located between the urethra and the ejaculatory ducts. It is closely related to the neck of the bladder above. Its ducts open into the urethra above the ejaculatory ducts (**Dauge et al., 1999**).

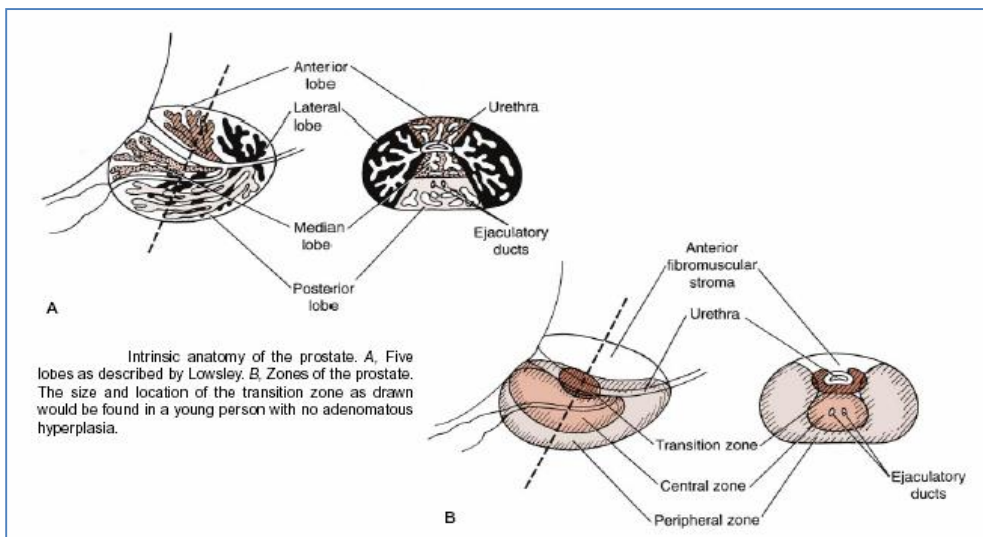


Figure 2 : Diagrammatic representation of the lobar and zonal anatomy of the prostate (**Rogers et al., 2002**).

Zonal Anatomy (McNeal)

McNeal established the current and most widely accepted concept of various zones rather than lobes of the prostate stating that the human prostate gland is a composite organ made up of several glandular and non-glandular components.

McNeal J.E. (1981) described four basic anatomic zones on the basis of biological and histological concepts. Each zone originates from prostatic urethra and has specific architectural features. These major glandular regions of prostate are labeled as the peripheral zone, the central zone, the transitional zone and the peri-urethral zone (**Grenier and Devonec, 2006**).

Table (1) describing the zonal anatomy of the prostate and its percentages, coincides with young men, however, in elderly this configuration changes such that the inner gland hypertrophies (BPH) and the peripheral zone remains static (**Patel and Rickards, 2002**).